This version of the article has been accepted for publication in *International Journal of Adhesion and Adhesives* after peer review and is subject to Elsevier's terms of use, but is not the Version of Record and does not reflect post-acceptance improvements, or any corrections. The Version of Record is available online at: https://doi.org/10.1016/j.ijadhadh.2022.103282

Role of surface structures on long term stability of adhesive joints between Ti-15V-3Cr-3Sn-3Al and polyether-ether-ketone

Miriam LÖBBECKE[1,*], Tolga J. BAYERBASI[1], Marion BARTSCH[1], Jan HAUBRICH[1]

[1]Institute of Materials Research, German Aerospace Center (DLR), Linder Hoehe, D-51147 Cologne, Germany

* Corresponding author: Miriam.Loebbecke@dlr.de

Abstract

Adhesive bonding of similar and dissimilar materials is a key enabler for lightweight design in the automobile as well as aerospace industries. The strength and durability of adhesive metal-polymer joints in humid atmospheres depends strongly on surface pretreatments. Different pretreatments of Ti-15V-3Cr-3Sn-3Al (Ti15-3) for joining to polyether-ether-ketone (PEEK) were investigated in order to optimize the joint properties and elucidate underlying bonding mechanisms. Micro- and nanostructured surfaces were created with laser and chemical pretreatments and characterized with microscopy and X-ray photoelectron spectroscopy (XPS). The mechanical performance of the joints was analyzed with single lap shear tests in both the initial condition and after hydrothermal aging. Without significant structuring only physico-chemical interactions were present that accounted for strengths of up

to 45 MPa. In the presence of micro- or nanostructures that add interlocking possibilities to the bonding, a maximum strength of 74 MPa was obtained. Hydrothermal aging resulted in poor residual strengths for samples without structuring, showing that humidity strongly degraded physico-chemical bonding. High aging resistance was particularly reached for laser pretreated specimens with an open-porous nanostructure. By comparing the different surfaces, it was found that (i) nanostructuring has a bigger impact on the aging resistance than microstructuring, and (ii) aging can be assigned mainly to weakening of physico-chemical bonding. Therefore, it can be deduced that nanomechanical interlocking is a key for producing long-term stable Ti15-3/PEEK joints.

Keywords: surface treatment, surface roughness/morphology, hybrid joints, aging, bonding mechanisms

1 Introduction

Adhesive bonding is an enabler for modern lightweight design in the automobile and aerospace industries. Similar and dissimilar materials can be bonded with thermoset or thermoplastic adhesives or assembled to composite materials such as, e.g., fiber-metal laminates by using the polymer matrices [1-6]. While in ground-based transport mostly glass, polymer, aluminum and steel parts are joined [6-8], aerospace applications also include bonding of titanium for structural parts (e.g., leading edges on GE90 and GEnx fan blades) [1-3, 5, 9, 10].

A major challenge for the reliability of adhesive joints are the mechanical and environmental loads that a component typically faces [1, 4, 9]. Particularly, fatigue loads and corrosive media including humidity often reduce the performance during service [9, 11-15], which in aeronautic applications has led to the extensive use of additional “fail-safe” rivets [5, 16].

In order to achieve suitable joint properties including a high degradation resistance against humidity, surface pretreatments of the bonding partners are employed [1, 9, 17]. Electrochemical anodization, plasma or laser treatments allow for long-term, aging resistant bonding and lead to the formation of micro- and nanostructured surfaces with oxidic character [1, 6, 11-13, 15, 17-19].

The effectiveness of the pretreatments depends strongly on the underlying bonding and aging mechanisms. Damage can occur due to debonding, interfacial changes of surface morphology and chemistry (e.g. hydroxylation on aluminum alloys or bond line corrosion [10, 18, 20] or due to swelling, plasticisation or even hydrolysis of the polymer (e.g., in polyamides [1, 17]). While adhesive bonding has already been studied for almost a century, the fundamental mechanisms of bonding and degradation are, in many cases, still poorly understood.

Generally, both mechanical as well as chemical bonding, or more exactly physico-chemical bonding mechanisms are known in metal-polymer joints. They depend on the nature of the joint surfaces, i.e. their chemistry and their morphology at different length scales, as well as on the properties of the polymer (e.g. visco-elastic behavior or water uptake) and its chemical functionalization ([1, 17, 18] and refs. therein). Mechanical bonding is based on polymer interlocking with rough surface structures at the micro- [21, 22] or nanometer level [1, 10-12, 14, 15]. Physico-chemical bonding of organic molecules to metal or oxide surfaces can derive from covalent, electrostatic, coordinative, π-interactions, hydrogen or dispersive Van-der-Waals interactions (hereafter referred to simply as "chemical" interactions/bonding) that vary substantially in strength [23, 24]. Sufficiently attractive chemical interactions are a prerequisite for good wetting of surfaces by a polymer and, thus, for the infiltration of rough surface structures giving rise to mechanical interlocking.

The relative importance of mechanical interlocking at the micro- and nanometer scales and chemical bonding has, however, remained a matter of debate. The contributions must vary for different systems and stretch from mechanical interlocking [11, 12, 14, 25-27], to physico-chemical bonding [1, 11-13, 15, 21, 26, 28]. The mechanical interlocking of a polymer by infiltration of open-porous nanostructures is nowadays often proposed as a reason for the enhanced long-term stability of joints against hydrothermal degradation such as for example in case of laser pretreated titanium joints [11, 12, 14]. Similarly, spongy nanostructures that are created by, e.g. chromic acid anodization (CAA) [29] or NaTeSi anodization [15], may allow for significant mechanical interlocking, although the latter study found more evidence for chemical contributions to the bonding.

Generally, chemical interactions must contribute to some degree to the bonding and its durability as evidenced for example in the case of an epoxy polymer on untreated titanium surfaces [11]. For some materials, e.g. PETI-5 on Ti-6Al-4V [13] or epoxy on commercially

pure (CP) titanium [26], chemical interactions may even exceed that of mechanical interlocking, especially in the initially bonded condition. Harris and Beevers, investigating steel or aluminum bonded with an epoxy (Araldite) after grit blasting, concluded that chemistry played a larger role than mechanical interlocking from the absence of a direct correlation between roughness and strength [21]. Earlier, also Chawla found that mechanical interlocking corresponds to much weaker bonding compared to chemical interactions [30]. Davids et al. even stated that the role of roughness is often misunderstood in terms of mechanical interlocking and that bonding with structural adhesives is generally of a chemical nature [4]. In that sense, roughness increases the surface area of a joint and hence, the available (chemical) bonding sites for the polymer.

In general, numerous studies agree in attributing strength reduction due to aging by humidity to weakening of the chemical bonding [4, 11, 15]. The aging effects are known to be more pronounced for thermoplastic- compared to thermoset-metal joints since the former commonly show a higher degree of interfacial failure [31, 32]. However, contrary to an often-presented belief, many thermoplastics can also bond strongly due to their chemical functionalities (e.g. aldehyde or keto-groups as found in polyether-ketone/PEK or polyether-ether-ketone/PEEK), which can interact sizably with cationic surface sites such as present on pretreated and thus oxidized titanium surfaces (e.g., Ti^{4+}) as evidenced from model catalysis [33-35].

Not surprisingly, also the proposed roles of the surface pretreatments cover a large spectrum and vary from cleaning and creating roughness [14, 25, 27] to purely increasing surface area and chemical activation [4] or a combination of both [1, 11, 12, 21, 31]. Therefore, advancing the understanding of the roles of surface morphology and chemistry for the bonding and damage mechanisms is essential for furthering surface pretreatments and adhesive joining: *Is*

mechanical interlocking crucial or chemistry? Does microstructuring add significantly to the joint strength and durability, or is nanostructuring decisive?

In order to elucidate these questions for a model titanium-thermoplastic system, experiments have been carried out with Ti-15V-3Cr-3Sn-3Al and PEEK to systematically vary the surface morphologies and study the effects on the bonding and aging behavior. Pretreatments have been chosen accordingly and characterized with dedicated surface analysis tools. In conjunction with accelerated aging experiments and lap shear testing of pristine and aged joints, the predominant factors for the bonding mechanisms have been studied.

2 Experimental

2.1 Materials

The metastable β-titanium alloy Ti-15V-3Cr-3Sn-3Al (Ti15-3; TIMET GmbH) was selected due to the good cold workability and therefore availability of thin foils, which, for instance, makes this alloy an interesting candidate for applications in fiber-metal-laminates. From 1.6 mm thick rolled sheets, strips were water jet cut and cleaned in acetone. The strips were bonded to single lap shear (SLS) specimens using the aviation certified semicrystalline thermoplastic polymer polyether-ether-ketone (PEEK; LITE TK; Lipp Terler GmbH, foil thickness 100 µm).

2.2 Sample preparation

2.2.1 Laser pretreatment

Prior to bonding, the titanium surfaces were laser pretreated with a pulsed Nd:YAG laser "CL20" (Clean-Lasersysteme GmbH, Herzogenrath) with a maximum power of 20 Watts, a wavelength of 1064 nm, pulse length of 110 ns, and a Gaussian laser profile (spot

diameter: ~65 µm) to structure the surfaces on the micro- and nanometer scales. Surface structures were modified by adjusting the laser process parameters of power, frequency, and scan speed. Varying power and frequency led to different laser pulse energies but only slightly different micro- and nanostructures, whereas a variation of laser scan speed allowed for the creation of pronounced microstructural differences. The line distance was kept constant at 45 µm. The investigated laser parameter sets are listed in Table **1**.

Table 1

Investigated laser parameter sets.

label (treatment)	power P [W]	frequency f [kHz]	scan speed V [mm/s]
L_{mE}	13.2	70	3000
L_{hE}	20.0	40	3000
$L_{mE\text{-}mV}$	13.2	70	500
$L_{mE\text{-}lV}$	13.2	70	200

Legend: L: laser treatment; E: laser pulse energy; V: scan speed; h: high; m: medium; l: low

2.2.2 Etching preparation

Etching treatments were used to remove or to change the laser-generated nanostructures. Two etchants were employed on untreated and laser pretreated surfaces to modify the nanostructure without affecting existing microstructures:

(i) KELLER solution (0.2 wt% HCl, 0.24 wt% HF and ~0.8 wt% HNO_3 in aqueous solution) was used to remove an existing nanostructure in laser structured surfaces.

(ii) A potassium hydroxide/hydrogen peroxide solution (40 wt% KOH solution/30 wt% H_2O_2 solution/H_2O: 30 ml/30 ml/40 ml for untreated surfaces; 30 ml/15 ml/55 ml for laser-treated samples) was used to create a nanostructure that differs in morphology from the laser induced structures.

Etching time and composition of the etching solutions were adjusted for optimal removal or generation of nanostructures (Table **2**).

Table 2

Combinations of laser and etching pretreatments used in this study to obtain different surface structures.

label (treatment)	**laser treat-ment**	**etchant; etching time**	**expected surface structure**
KEL	none	KELLER; 15 s	none
KOH	none	KOH/H_2O_2; 120 s	nano
L_{mE}-KEL	L_{mE}	KELLER; 30 s	micro
L_{mE}-KOH	L_{mE}	KOH/H_2O_2; 120 s	micro/nano
L_{mE-mV}-KEL	L_{mE-mV}	KELLER; 90 s	micro

Legend: L: laser pretreatment; E: laser pulse energy; V: scan speed; h: high; m: medium; l: low; KEL: etching treatment with KELLER solution; KOH: etching treatment with potassium hydroxide solution.

2.2.3 Bonding and aging

The pretreated Ti15-3 strips (72.5×10 mm², thickness 1.6 mm) were bonded with PEEK to form SLS specimens with an overlap area of ca. 5×10 mm². Bonding was performed in ambient air in a laboratory furnace P330 (Nabertherm) at ca. 395 °C. The furnace program was selected in such a way that the target temperature was above the melting temperature of PEEK (T_m = 343 °C). The temperature was maintained for at least 15 min (Fig. 1), so that the polymer could infiltrate the surface structure of the titanium sheets in the molten, low-viscosity state. The bonding area was subjected to a weight of 72 g resulting in a low pressure of 7.2 mbar.

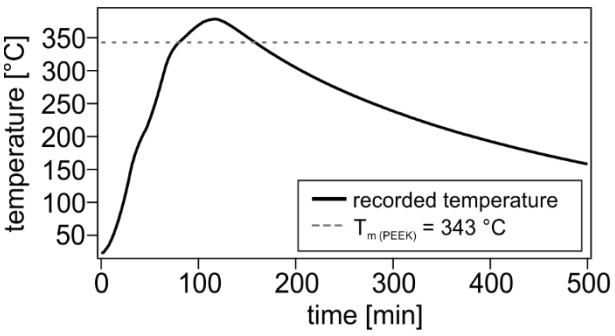

Fig. 1: Time vs. temperature for the PEEK bonding procedure. The recorded temperature as well as the melting temperature of PEEK is shown.

The specimen dimensions and overlap area were intentionally reduced compared to the German standard DIN EN-1465 since preliminary experiments showed very high lap-shear strengths of around 80 MPa. By reducing the overlap area significant plastic deformation of the 1.6 mm thick metal strips can be avoided, as to be otherwise expected for standard sized 25×12.5 mm^2 joint areas given a yield strength of ~1000 MPa for Ti15-3. The reduced joint length can lead to an increase of the lap shear strengths, due to a decrease of the local stress peaks at the edges, with respect to the values expected from larger joints. Since yielding and bending effects would lessen the merit of the mechanical tests, they were deemed more critical, and therefore, the joint area was reduced.

For each set of laser parameters/etching treatments 6 single lap shear specimens were produced. A set of 3 SLS samples for each surface pretreatment and condition was aged for 7 days in 80 °C hot deionized water prior to testing.

2.3 Mechanical testing – single lap shear tests

SLS tests were conducted according to DIN EN-1465 with pristine and aged samples. The specimens were mechanically clamped and loaded in tensile mode with an Instron universal testing machine (model 5566A) with a displacement rate of 1 mm/min until failure occurred.

The loads were measured with a 10 kN load cell (model 804, series 2525). The joint strength (maximum SLS strength) was calculated from the maximum load and the true adhesion area. The adhesion area was determined by averaging the bonded areas on the two resulting fracture surfaces as measured with a stereo-microscope (SteREO Discovery V12, Zeiss). The ratio between the strength after aging and the initial strength was defined as aging resistance.

2.4 Surface and fracture surface analysis

2.4.1 Microscopic methods

The topography of different surface structures was characterized with a Zeiss LSM 700 (laser λ = 405 nm) confocal laser scanning microscope (LSM). Tile scans (250×250 μm^2) were conducted at a 500-times nominal magnification with a 12.1 mm pinhole setting. 3D-heightmaps were recorded, and the 3D roughness parameters S_{dr} (developed interfacial area ratio – surface enhancement), S_z (maximum height), and S_a (arithmetic mean height) were computed with the Zeiss ConfoMap software.

Pre-treated Ti15-3 surfaces and fracture surfaces of the lap shear specimens were investigated in detail by scanning electron microscopy (SEM). The surface structures on different length scales were recorded with a Zeiss Ultra 55 field emission SEM (primary beam energy: 5 keV; working distance: ~8 mm) in secondary electron mode (Everhart-Thornley detector), the different materials on a fracture surface were revealed with the backscatter electron detector mode. To avoid charging effects, Pt was deposited on the surface before investigation.

In order to obtain further insights into the morphology and elemental distributions of the nanostructures within the laser influenced zone, lamellae of selected laser pretreated titanium strips were prepared by focused ion beam (FIB) milling (dual beam FIB FEI Helios 600i) for investigations by transmission electron microscopy (TEM). The surfaces were covered by Pt and C protection layers with a sputter process to prevent damage by the ion milling procedure.

Afterwards the thinned lamellae (<0.5 µm, down to 0.05 µm) were transferred into a Philips Tecnai F30 analytical TEM. Dark field images were recorded to establish morphology information whereas energy filtered TEM (EFTEM) was used for the chemical elemental analysis.

2.4.2 X-ray photoelectron spectroscopy

The surface chemistry on the differently prepared titanium surfaces was analyzed using the surface-sensitive X-ray photoelectron spectroscopy (XPS). Since the escape depth of the detected electrons is small, XPS provides (unlike energy dispersive X-ray spectroscopy) information on chemical composition from the first few nanometers thickness of the surface region.

Ti15-3 sheets of 5×10×1.6 mm³ were cleaned, surface pretreated, and immediately sealed under a protective Ar atmosphere in order to transfer the specimens into the ultrahigh-vacuum XPS setup (SPECS PU-XR50). The samples were bonded with carbon-pads to stainless steel sample holders. A Mg-anode (Mg-K_α; E_{Photon} = 1253.6 eV) was used, and detailed photoelectron spectra of Ti, O, N, C, Al, V, Sn, Cr were recorded with a pass energy of 50 eV.

The qualitative analysis of the spectra was performed after removal of satellite peaks (which occurred since no monochromator was used), and fitting the respective backgrounds with the *Tougaard* four-parameter function [36]. Curve fitting was subsequently carried out with symmetric Voigt profiles.

The binding energies (BE) were referenced to the $Ti2p_{3/2}$ signal of TiO_2. The Ti2p system exhibited a splitting into two maxima with a difference in BE of ~5.7 eV (full width half maxima FWHM: $Ti2p_{3/2} \approx 2.4$ eV, $Ti2p_{1/2} \approx 2.7$ eV). Since the exact structure of the TiO_2 (presumably disordered, non-equilibrium surface structures can be expected after laser treatments) was unknown, the thermodynamically most stable, fully oxidized TiO_2(110)

surface of rutile was chosen as reference and the BE set at 459.2 eV [37]. Lower titanium oxidation states (see e.g. ref. [38]) can easily be identified by their BE positions relative to the Ti2p signal for TiO_2 that is always unambiguously assignable. No charging effects occurred due to the thin-film nature of the oxide layer on pretreated titanium samples, which was confirmed by the absence of peak-shifts over the scan time. The spectra of the elements V, Sn, and Cr exhibited very low signal intensities and could not be analyzed.

3 Results and discussion

3.1 Surface structure variation by laser treatment

3.1.1 Surface analysis

Micrometer-sized laser structures are generated by the laser on the Ti15-3 surfaces, which have been varied from rather flat morphologies to deep trenches by changing the laser scan speed (Fig. 2 (a-e)). In comparison with untreated titanium sheets, the laser treated surfaces show a high micro-roughness and waviness. Regular overlapping but distinctly recognizable structures are formed (max. height ca. 20 µm; Table 3) associated to the laser pulses L_{mE} and L_{hE} (V = 3000 mm/s) [19]. Decreasing the scan speed ($L_{mE\text{-}mV}$ and $L_{mE\text{-}lV}$) leads to sizable roughness increases upon formation of deep trenches and grooves (Table **3**; Fig. 2 (d-e)). However, LSM only provides information on the microstructures, whereas structuring in the lower nanometer regime cannot be characterized with this technique.

Table 3

Roughness parameters S_z, S_a, and S_{dr} for differently laser pretreated Ti15-3 surfaces determined by means of LSM.

treatment	**S_z [µm]**	**S_a [µm]**	**S_{dr} [%]**
untreated	11.8	0.8	10.4

L_{mE}	19.8	1.1	17.3
L_{hE}	20.6	1.4	15.2
$L_{mE\text{-}mV}$	34.1	6.2	81.9
$L_{mE\text{-}lV}$	48.7	14.1	213.0

The SEM images reveal that all laser generated microstructures are fully covered by fine nanostructures that differ in size and shape (Fig. 2 (g-j)). The nanostructures generated by medium pulse energies (L_{mE}; Fig. 2 (g)) appear very regular and globular; they are coarser at low scan speeds (Fig. 2 (i-j)). In contrast, the L_{hE} nanostructure seems to be more heterogeneous (Fig. 2 (h)).

The thickness and composition of the layers at the interface were characterized for the L_{me} and L_{hE} case by TEM (Fig. 3). The L_{mE} nanostructured layer is relatively thin with a height of around 80 nm (Fig. 3 (a, b)), whereas the L_{hE} generated layer measured up to 200 nm (Fig. 3 (c, d)).

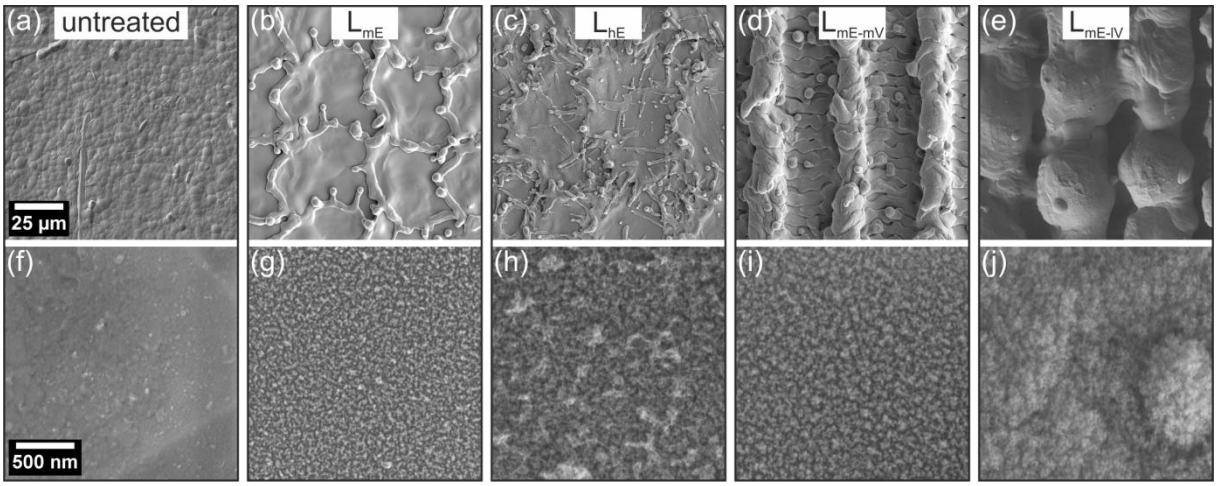

Fig. 2. SEM images of the pretreated Ti15-3 surfaces at µm-level (a-e) with the related image on nm-level placed below (f-j). The corresponding laser treatment parameters are provided at the top.

All analyzed nanostructures created by the laser consist of titanium oxides (Fig. 3 (a, c): Ti and O signal, Fig. 3 (b, d): EFTEM Ti signal only). The distribution of titanium and its oxides, respectively, reveals differences between the nanostructures of L_{mE} and L_{hE} treated surfaces in detail: both titanium oxide layers have an open porous character, but comparing the L_{mE} and the L_{hE} generated nanostructures, the latter is much more branched. Further information is provided by the detected carbon signals, which stem either from the carbon protection layer (Fig. 3 (a)) sputtered on laser treated sheets which were not joined to SLS test specimens or from the infiltrated polymer, when the TEM sample was prepared from an SLS specimen (Fig. 3 (c)). The latter TEM image indicates an excellent wetting and infiltration behavior of PEEK into the nanostructure.

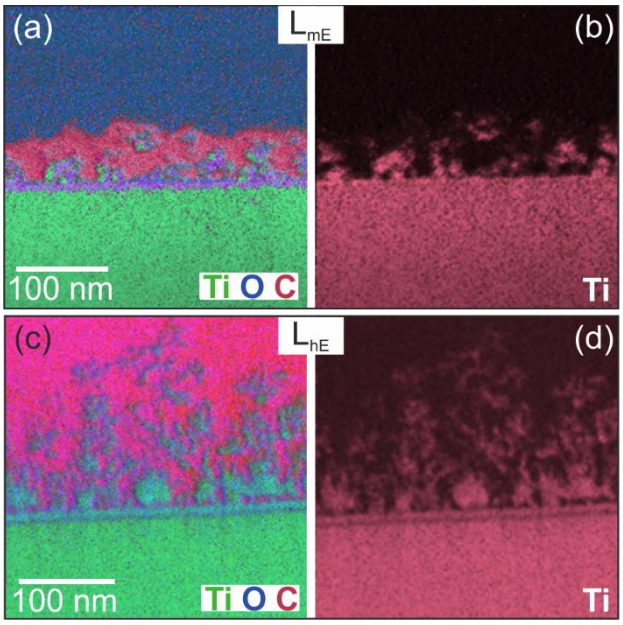

Fig. 3. Color-coded EFTEM maps of TEM lamellae of two laser treated Ti15-3 surfaces. (a, c): superimposed Ti, O and C signals; (b, d): extracted Ti signal for better visibility of the morphology of the laser-induced nanostructures.

In order to further analyze the chemical composition of the surface region of the nanostructures obtained after laser treatment and to identify chemical binding sites, XPS was employed. Representative XPS spectra are shown in Fig. 4. For sake of brevity, only for two

different laser-treated surfaces XPS spectra are displayed, since the XPS spectra of the other investigated surfaces showed very similar intensity distributions. The Ti2p and O1s spectra are sufficient to describe qualitatively the similarities and differences with respect to the main chemical components for both exemplary surfaces. The relative intensities, as well as positions and shape of the intensity peak envelopes are similar in the case of the Ti2p for L_{mE} and $L_{mE\text{-}mV}$ (inset of Fig. 4 (a)), since the main oxidation stage of the titanium is +IV in each of the nanostructure layers ($Ti2p_{3/2}$ was fixed at 459.2 eV [37] as described in Section 2.4.2).

The main O1s component for lattice TiO_2 oxygen atoms (six-coordinated bulk and five-coordinated surface oxygen atoms) is generally associated with the most intense oxygen peak and detected at 530.6 eV (Fig. 4 (b)) in agreement with literature [39]. Higher BE components within the O1s spectra (indicated by different thin lines in Fig. 4 (b)) belong mostly to organic contaminations (~532.1 eV, [39, 40]), hydroxyls (~532.1 eV [39-41]), and water (molecular adsorbed ~533.5 eV; physisorbed >535 eV [39, 41]), which were likely present on all investigated surfaces due to the handling and preparation of samples in air (unlike highly clean ultra-high vacuum conditions typically used in surface science). The ubiquitous organic contaminations were evidenced by the C1s data (Fig. 4 (c)). However, the O1s component around 531/532 eV [40] can also be correlated with surface Al_2O_3, which due to the low surface energy may form by preferential segregation of aluminum during the film formation. Slight differences in the relative intensities of the higher O1s BE components were observed after different laser pretreatments, especially when comparing $L_{mE\text{-}mV}$ and L_{mE}, which may indicate a higher amount of organic contaminations and higher concentrations of aluminum oxides on the $L_{mE\text{-}mV}$ surface, respectively.

From the XPS data the conclusion can be drawn that the surface chemistry has not changed significantly with the variation of the laser pretreatment parameters. Thus, within this study

the structural changes on the micro- and nanoscales of the surfaces are the dominant factors influencing the mechanical joint behavior and its aging properties.

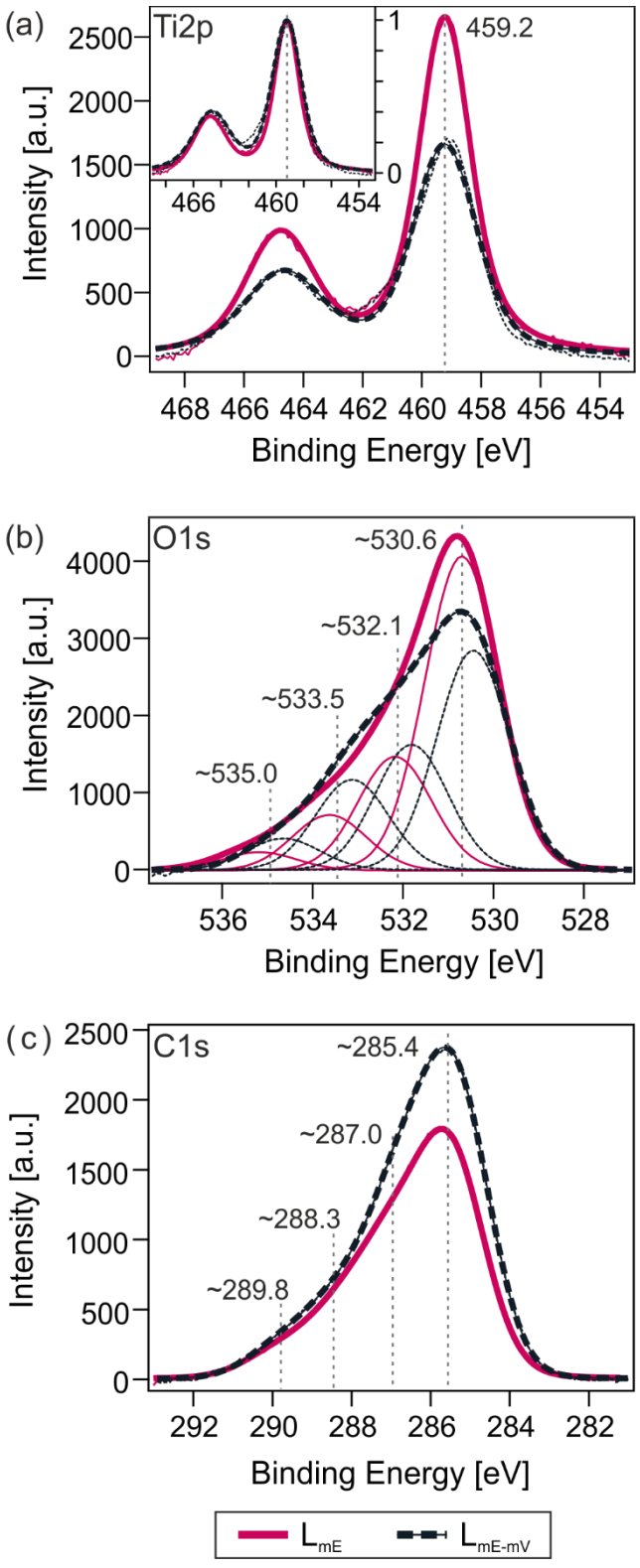

Fig. 4. XPS spectra of (a) Ti2p (Ti(IV) at 459.2 eV [37]) with normalized intensities in the inset diagram, (b) O1s with corresponding peak envelopes (BE components indicated by the thin lines) for two selected Ti15-3 surfaces laser treated using laser parameters L_{mE} and $L_{mE\text{-}mV}$ (E_{Photon} = 1253.6 eV), and (c) C1s spectra corresponding to the O1s results with subcomponents C-H, C-C (~285.4 eV), C=O, C-OH (~287.0 eV), COOR (~288.3 eV), carbonates (~289.8 eV) [40, 42, 43].

3.1.2 Mechanical characterization

The impact of the laser treatments and the resulting surface morphologies on the bond strengths is investigated by single lap shear tests. The results are summarized in Fig. 5. The mostly small standard deviations in the sample sets provides evidence of a high degree of reproducibility of the mechanical tests as well as of the laser surface treatments.

Initial SLS strengths, i.e., prior to aging, exceeding 45 MPa are reached (Fig. 5) even without surface treatment. Thus, if no significant surface structuring is present, physico-chemical interactions must play a sizable role in Ti15-3/PEEK joints at least in this initial, undegraded condition.

Much higher initial joint strengths of up to 74 MPa are achieved with the laser-treated samples. There are only small differences between the various laser treatments, showing that all laser generated surface structures lead to high initial bonding strengths. Importantly, the higher micro-roughness of the trenches formed by $L_{mE\text{-}mV}$ and $L_{mE\text{-}lV}$ (compare Table 3) does not lead to higher initial strengths. In fact, for the lowest scan speed ($L_{mE\text{-}lV}$), which resulted in the highest surface roughness, even slightly lower strength values (66 ± 2 MPa) were measured.

After accelerated aging in hot deionized H_2O (7 days at 80 °C) the residual bond strengths of all investigated samples are degraded to different degrees (Fig. 5). The residual strengths of

the untreated samples generally dropped critically to values below 15 MPa, resulting in a poor aging resistance of only 32%.

Among the different laser-treated samples – which all have a micro- and nanostructure – a variation of the strength after aging is observed: the residual strength is lowest for the surface treatment L_{mE} (46 ± 3 MPa, aging resistance: 62%), which generates the surface microstructure with the lowest roughness values for the maximum and arithmetic mean height and the least pronounced nanostructure.

All other laser parameter sets lead to higher residual strengths of 55-60 MPa. The high residual strengths and aging resistances (~80%) can be attributed to the pronounced nanostructures based on the above findings that large differences in microroughness had no distinct effect on the aging resistance (L_{mE} versus $L_{mE\text{-}lV}$), and the sample with the least pronounced nanostructure showed the lowest aging resistance (case of L_{mE}).

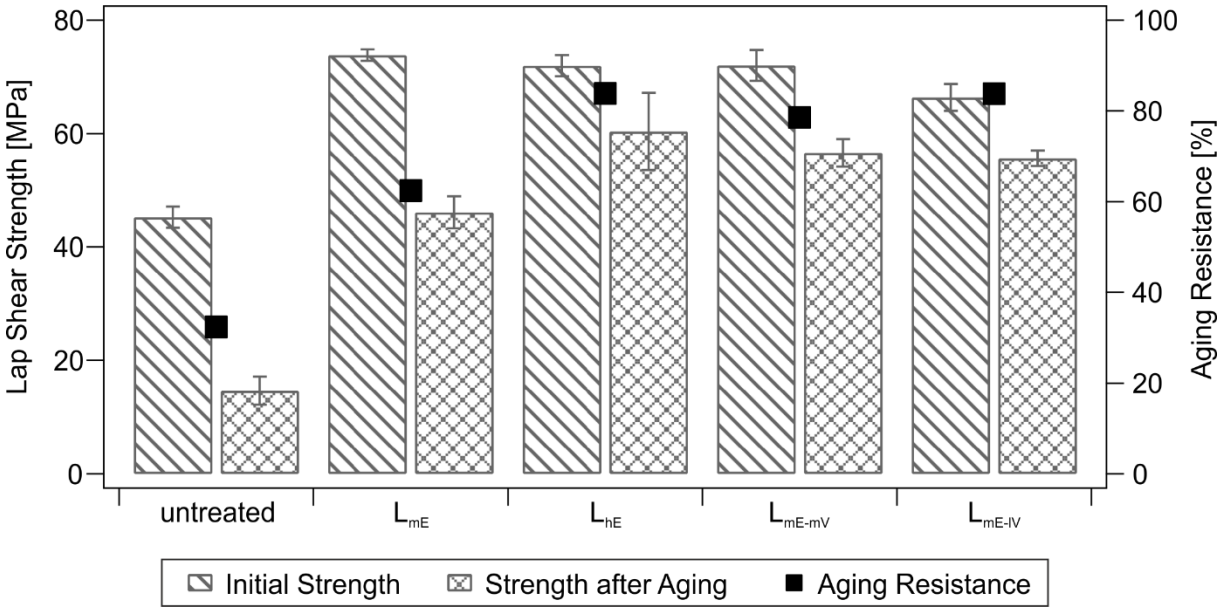

Fig. 5. Single lap shear strengths of untreated and laser-treated Ti15-3/PEEK specimens in the initial condition (initial strength) and aged condition (residual strength) are shown as well as the corresponding aging resistance.

3.1.3 Fractography

The fracture surfaces of the SLS samples were investigated to identify the weakest links within the differently prepared Ti15-3/PEEK joints by means of the failure pattern. In none of the cases did a failure occur within the oxide layer or at the interface between oxide and laser pretreated Ti15-3-substrates. Using SEM for a detailed analysis, all failures were found to be either adhesive at the interface between oxide and the polymer or fully cohesive within the PEEK.

The different failure modes are indicators for the bonding properties of the joints: a high fraction of adhesively failed regions was typically found for the joints exhibiting poor mechanical performance, i.e. especially the untreated samples (Fig. 6 region A and a).

Cohesive failure within the polymer was especially seen in the middle region of the SLS fracture surfaces (Fig. 6 region B and b, Fig. 7 region B and b), which indicates a strong connection between substrate surface and polymer. This is particularly true for the laser structured samples.

The cohesive failure can be divided into two different kinds: a “fully” cohesive failure in the polymer bulk region (Fig. 7 region B and b) as well as a cohesive failure within the polymer but very close to the interface, which occurred particularly at the edges of the bonded area.

This latter type can also be considered as “pseudo-adhesive” failure since, judged from optical microscopy, the failure is adhesive in nature as no polymer residues can be detected (Fig. 7 region A). Only when analyzing the fracture surfaces in the SEM (mainly in backscatter electron detector mode) it becomes obvious that the interface on the substrate side is still fully covered by a thin polymer layer (Fig. 7 region a), showing that this case is an intermediate type between “ideal” adhesive or cohesive modes.

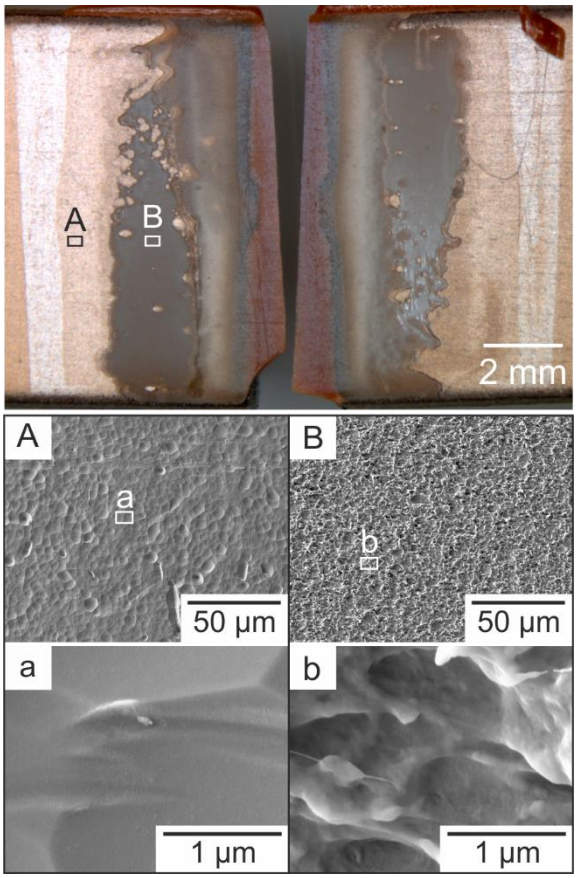

Fig. 6. Fracture surfaces of a Ti-15-3/PEEK SLS specimen without any surface treatment prior to bonding and no aging before testing (initial condition). The marked positions refer to the corresponding SEM images below.

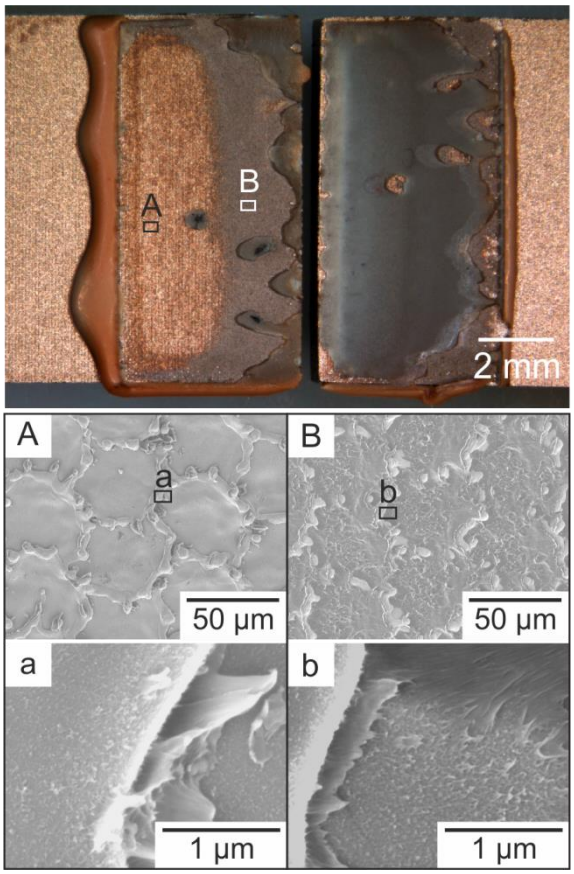

Fig. 7. Fracture surfaces of a Ti-15-3/PEEK SLS specimen (initial condition) treated with laser parameter L_{mE}. The marked positions refer to the corresponding SEM images below.

After aging of the specimens in 80 °C hot deionized water for 7 days, the fraction of these apparently adhesively failed areas increases for the untreated and the L_{mE} specimens with the minor expressed nanostructuring. The drop in the SLS strengths correlates well with this observation.

The correlation between failure loci and strength changes is less obvious for the laser treated samples with more expressed nanostructures. Here also a minor strength drop occurs due to aging, but the failure mode consistently remains cohesive in nature. This observation can potentially be explained by a weakening of the PEEK by water uptake (i.e., swelling [17]), so the bulk strength of the polymer may be lower after accelerated aging, thus leading to a lower overall joint strength.

3.2 Nanostructure variation by chemical treatment

3.2.1 Surface analysis

In order to modify the nanostructures of sample surfaces for tracing the changes observed in the joint properties back to the prevalent structuring, etching treatments have been used. Roughness measurements confirm the etching treatments only slightly affect the roughness and structures at the micrometer level (Table **4**): KEL and KOH (untreated), L_{mE}-KEL and L_{mE}-KOH (L_{mE}), and $L_{mE\text{-}mV}$-KEL ($L_{mE\text{-}mV}$). SEM shows that while the etchants had minor influence on the microstructure (Fig. 8 (a-e); the number of attached µm-sized particles might be somewhat reduced), the nanostructures are significantly affected by the etching treatment (Fig. 8 (f-j)).

Table 4

Roughness parameters S_z, S_a and S_{dr} for differently treated Ti15-3 surfaces measured with LSM.

treatment	**S_z [µm]**	**S_a [µm]**	**S_{dr} [%]**
KEL	6.9	0.4	4.3
KOH	9.5	0.7	8.8
L_{mE}-KEL	16.1	1.3	21.0
L_{mE}-KOH	13.6	1.3	20.5
$L_{mE\text{-}mV}$-KEL	30.9	6.0	152.0

The surface structures on nanometer level are modified qualitatively by the two investigated etching treatments: Existing nanostructures can be removed successfully by KELLER (Fig. 8 (f, h, j); Fig. 9 (a, b)) whereas the formation of a nano-sized, open-porous structure (thickness ~50 nm) is obtained with KOH/H_2O_2 (Fig. 8 (g, i); Fig. 9 (c, d)). The nanostructure caused by the KOH/H_2O_2 etchant has a distinctly different appearance compared to the laser induced nanostructure (cf. Fig. 2 (g)-(h) and Fig. 3). Note that the KOH/H_2O_2 nanostructure

on untreated (Fig. 8 (g)) and laser-treated (Fig. 8 (i)) surfaces are surprisingly also slightly different. This may be due to different pre-conditions on both substrates (i.e., structure, oxide layer, organic or possible residual contaminations) and, hence, the reactions between the Ti15-3 (oxide) surface and etchant.

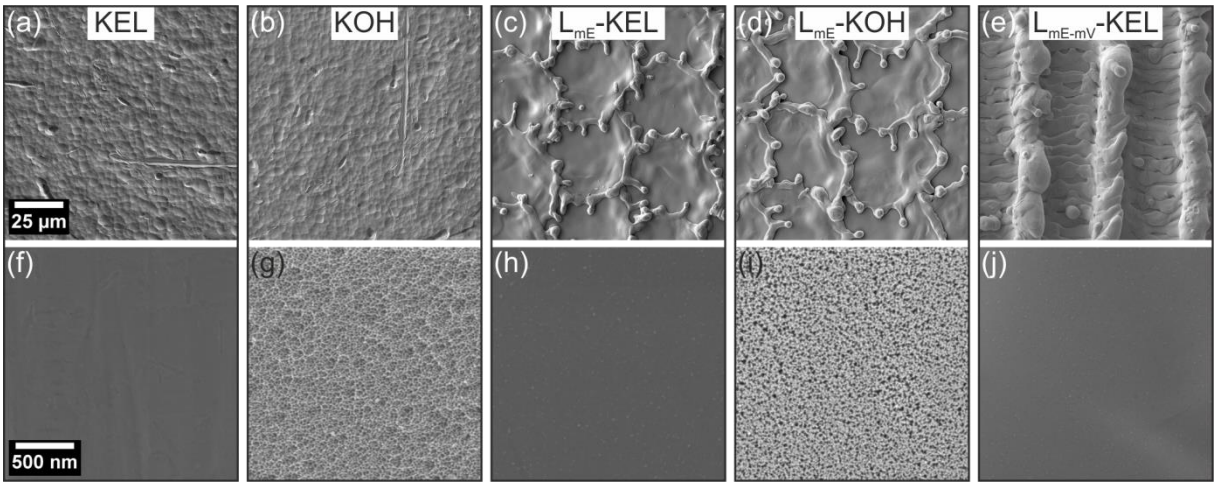

Fig. 8. SEM images of the laser treated and etched Ti15-3 surfaces at micrometer (a-e) and nanometer level (f-j). The etchants and laser treatment parameters are provided at the top.

EFTEM shows that the chemically etched Ti15-3 surfaces are covered mainly with titanium oxides (Fig. 9 (a, c): EFTEM Ti and O signals), very similar to the purely laser treated specimens (cf. Fig. 3). The C signals in Fig. 9 originate from the C protection layer deposited on the pretreated specimen prior to TEM lamella preparation.

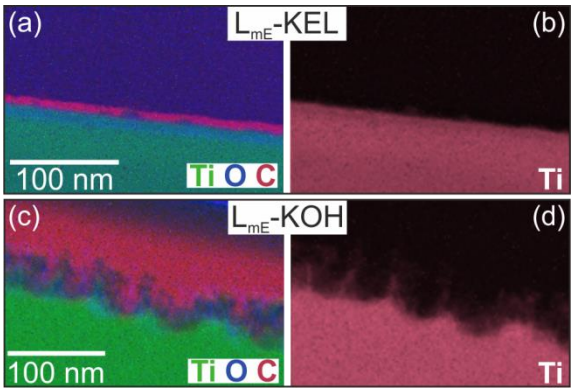

Fig. 9. Color-coded EFTEM maps of TEM lamellae of laser-treated and etched Ti15-3 surfaces that were subsequently coated with C. (a, c): superimposed Ti, O, and C signals; (b, d): extracted Ti signal of the KOH/H_2O_2 etched nanostructures.

The XPS investigations of the etched but not laser-treated surfaces reveal that the chemical composition of the surface layer remains unaffected by the etching procedures. The position of the $Ti2p_{3/2}$ peak at 459.2 eV matches in all cases that of Ti(IV) in TiO_2, confirming that surface chemistry of the etched surfaces is not changed (Fig. 10).

For L_{mE}-KEL, however, additional peaks occur at BE lower than the Ti^{4+} component in the Ti2p XPS spectrum, indicating the presence of lower oxidation states. A peak observed at ~454.4 eV corresponds to metallic Ti(0) [40]. The other subcomponents can be associated to Ti(III) at ~458.2 eV, Ti(II) at ~456.7 eV and Ti(I) at 455.4 eV (Fig. 10) (a)), which is in good agreement with [38]. Thus, it can be assumed that a layered structure within the information depth of XPS is detected consisting of a TiO_2 top layer below which intermediate layers of oxides of lower oxidation states form. On all other specimens in this study the TiO_2 layer was too thick (more than a few nm) to detect the lower oxidation states or even the metallic substrate below with XPS.

The O1s spectra of Keller etched surfaces indicate the presence of adsorbed species on these samples in addition to the lattice TiO_2 oxygen (Fig. 10) (b)). The lattice oxygen signal of titanium oxide at ~530.5 eV is the largest contribution, consistent with the O1s spectrum of

the laser treated L_{mE} sample (cf. Fig. 4 (b)). No components associated with lower Ti oxidation states are found at lower BEs in the O1s data.

Apparent is a basic difference between KELLER and KOH/H_2O_2 etched surfaces. The envelopes of O1s spectra of the KELLER treated surfaces with and without prior laser treatment (KEL, L_{mE}-KEL) are shifted towards higher BE. This signifies larger contributions of either organic contaminations caused by an uncomplete removal of the KELLER-etchant after the treatment or increased fraction of components in the typical BE range for hydroxyls and water (533-536 eV; cf. Section 3.1.1).

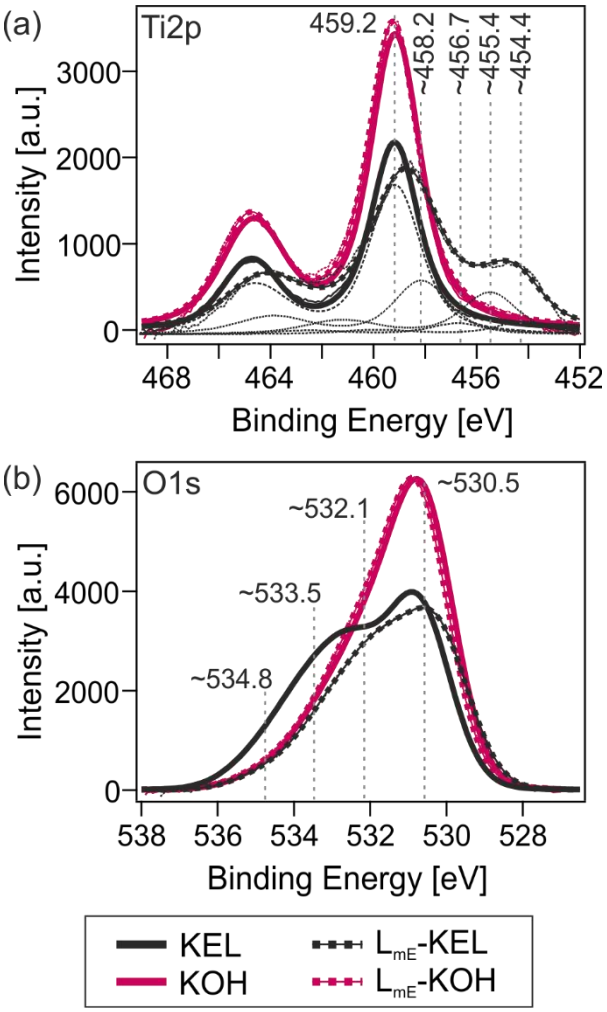

Fig. 10. XPS (a) Ti2p and (b) O1s spectra of laser treated and etched Ti15-3 surfaces (E_{Photon} = 1253.6 eV); thin black lines in (a) correspond to the peak envelopes associated to different Ti oxidation states for L_{mE}-KEL.

3.2.2 Mechanical characterization

The effect of the different surface structures on the bond performance is investigated by SLS tests. The standard deviations of the SLS strength are generally larger for the etched than for the laser pretreated samples (Fig. 11 vs. Fig. 5). The lower reproducibility of chemical treatments (differences due to varying etchant composition, etching time, surface contaminations, flushing and drying after etching etc.) compared to the more reproducible laser treatments becomes obvious.

All of the initial surface conditions lead to a certain basic initial SLS strength, which amounts to at least 48 ± 8 MPa (lowest for KEL; Fig. 11). Higher initial SLS strength values are measured for the structured surfaces, independent of the size-scale of the structures: very similar initial strengths are measured for KOH (64 ± 6 MPa; nanostructure only), L_{mE}-KEL (62 ± 2 MPa; microstructure only), and L_{mE}-KOH (67 ± 3 MPa; micro- and nanostructure). Even higher SLS strengths are reached for the more pronounced surface microstructure of $L_{mE\text{-}mV}$-KEL (76 ± 1 MPa; microstructure only; Fig. 11).

The residual SLS strengths after aging depend to a larger extent on the morphology of the surface structure. Without any surface structures (KEL) the SLS strength decreases below 20 MPa after aging (aging resistance: 42%).

The SLS strengths after aging of the samples with surface microstructures are strongly dependent on their morphology. L_{mE}-KEL is characterized by the lowest SLS strength values after aging (6 ± 4 MPa) despite the presence of the microstructure formed by melt-craters and rims. This SLS strength corresponds to an aging resistance of merely 9%. The more pronounced melt microstructure, which formed when lowering the laser scan velocity ($L_{mE\text{-}mV}$-KEL) prior to the Keller etching, leads to a higher aging resistance (56%). The residual SLS strength of 43 ± 6 MPa is comparable to the values for L_{mE}, but lower than that for the

same microstructure with nanostructure ($L_{mE\text{-}mV}$: 57 ± 2 MPa). Removing the nanostructure by Keller reveals a highly nonlinear dependence of the aging resistance on the microstructure with least aging resistance for a moderate roughness.

The combination of laser-induced microstructure and nanostructure from KOH/H_2O_2 etching (L_{mE}-KOH) leads for moderate microstructure roughness to significant residual strengths of 42 ± 4 MPa (aging resistance: 62%). Hence, the chemically formed nanostructure seems to be as suitable as the laser-induced nanostructure of L_{mE} (Fig. 11, compare to Fig. 5) for obtaining a long-term resistant bond.

Surprisingly, the samples that are covered only by the nanostructure from KOH/H_2O_2 etching but no microstructure possess quite low SLS strengths of only 20 ± 7 MPa after the aging. Assuming that this is correlated only with the bonding and that wetting and infiltration are unaffected, the mere presence of a nanostructure seems not to be sufficient for an improved aging resistance. One possible origin for the weakening of the bonding may arise from hydrothermal reordering or recrystallization of the titania oxide films [44-46], either laser-generated or formed by etching, which will be discussed in detail in section 3.3.

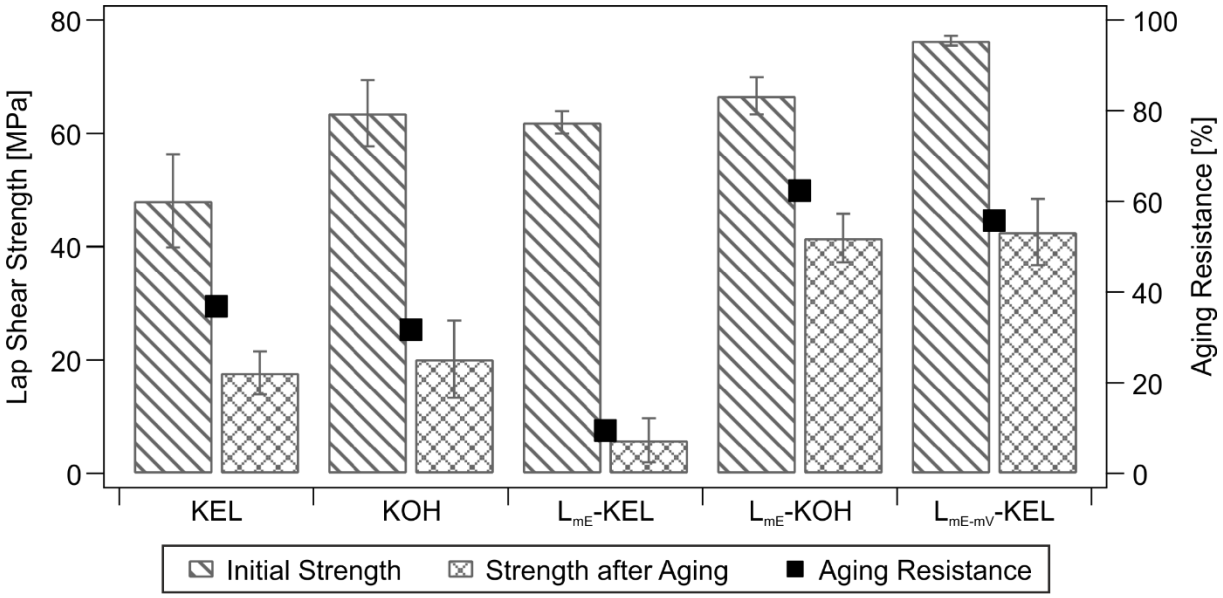

Fig. 11. Results of single lap shear tests. Strengths of specimens in initial condition (initial strength) and aged condition (residual strength after aging) are shown as well as the aging resistance of Ti15-3/PEEK samples with different surface treatments.

3.2.3 Fractography

The appearance of fracture surfaces of the etched samples depends on the surface structures induced before joining. If the sample surface has no nanostructure nor microstructure (i.e., KEL), mostly adhesive failure is observed both for the initial and aged conditions. Whenever a microstructure exists (L_{mE}-KEL, L_{mE-mV}-KEL), larger fractions of polymer remain on the fracture surface, in particular at undercuts of the microstructures (Fig. 12 (a) region A), which implies cohesively failed regions. The more pronounced the microstructure is, the more polymer remains at the surface and thus the higher the contribution of the cohesive failure is. On the flat parts of the surface between the melt pool rims of the microstructures, little polymer is left as evidenced by LOM and SEM.

Obviously, the presence of the microstructure alone is not a guarantee for durable mechanical interlocking under humid service conditions: aged L_{mE}-KEL samples with moderate surface roughness show almost purely adhesive failure patterns (Fig. 12 (b) region B). The prevalence

of adhesive failure is in accordance with the poor aging resistance of the KELLER etched samples (L_{mE}-KEL: 9%). Samples with pronounced surface microroughness ($L_{mE\text{-}mV}$-KEL) show a medium aging resistance of almost 60% despite a mainly adhesive failure. This can be attributed to the characteristic corrugated surface microstructure (cf. Fig. 9 (e)): large adhesively failed areas without polymer residue lie in flat areas between the linear rims, whereas a lot of PEEK remains at undercuts of the rims, indicating localized cohesive fracture and hence leading to the medium SLS strength after aging.

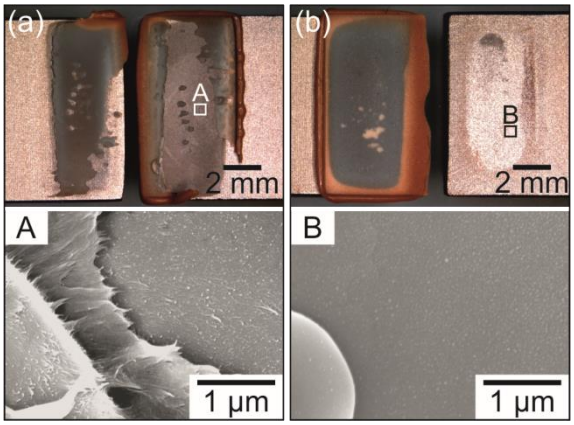

Fig. 12. Fracture surfaces of an SLS specimen (Ti15-3/PEEK) with surface treatment L_{mE}-KEL in (a) initial and (b) aged condition. The marked positions refer to the corresponding SEM images below.

A different picture results in case of the fracture surfaces of the KOH/H_2O_2 treated specimens. The surfaces are almost fully covered by PEEK, indicating that a cohesive failure mechanism prevails. PEEK not only remains at undercuts of the surface microstructure but also on flat but nanostructured surface areas (Fig. 13). The polymer adhering at nanostructured surfaces has cohesively failed near the interface between substrate and polymer, thus the etched surface structure becomes visible in the SEM again (pseudo-adhesive failure). After aging only few adhesively failed areas were identified on the L_{mE}-KOH fracture surfaces near the edges of the joints (Fig. 13 (b)), where high stresses occur. The observed fracture mode of L_{mE}-KOH is

consistent with the medium strength after aging and corresponding medium aging resistance. In the case of the KOH/H_2O_2 etched samples without microstructural surface features (KOH) mostly adhesive failure was observed, leading to low strength after aging. Even at high magnification SEM did not show that widely distributed polymer rests on the nanostructure. Only a few but large residues of polymer are visible on the nanostructure (Fig. 14).

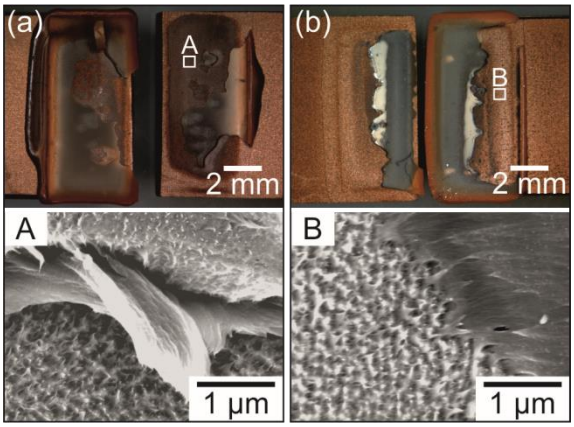

Fig. 13. Fracture surfaces of an SLS specimen (Ti15-3/PEEK) with surface treatment L_{mE}-KOH in (a) initial and (b) aged condition. The marked positions refer to the corresponding SEM images below.

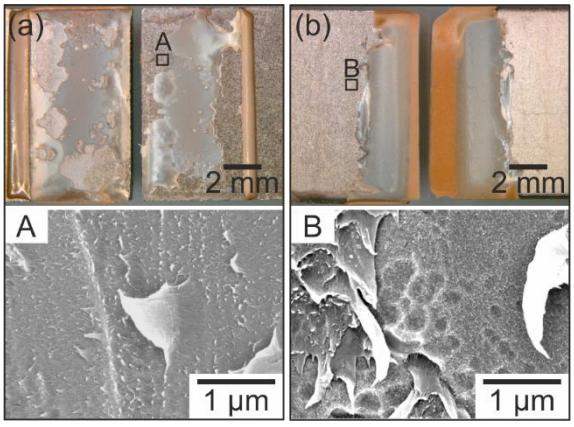

Fig. 14. Fracture surfaces of an SLS specimen (Ti15-3/PEEK) with surface treatment KOH in (a) initial and (b) aged condition. The marked positions refer to the corresponding SEM images below.

3.3 The role of surface structures

Surface structuring of the metallic substrate exerts a strong role for the investigated Ti15-3/PEEK joints. The involved chemistry of the surface oxide layer and the polymer as well as the surface topography generated prior to bonding are important for the bond strength and aging resistance and thus the joint performance.

Chemistry plays a role for all investigated surface conditions including the wetting behavior and infiltration into cavities or nanostructures. This is particularly evident from the SLS strength results on untreated (45 MPa) or KEL (48 MPa) samples that are unstructured, but reach sizable initial bond strengths by chemical interactions only. Additional surface structuring can lead to much higher SLS strengths (see Fig. 5; Fig. 11). Since the surface chemistry is not altered significantly by the various laser or chemical treatments (Section 3.1.1 and 3.2.1), but only the kind of surface topography, the different SLS strengths as well as their sensitivity to humidity must be mainly due to the changing structural characteristics of the surface, especially the morphology of micro- and nanostructures. On the one hand, the structuring leads to a surface enhancement and hence more potential binding sites for an increased number of chemical interactions. On the other hand, the structures enable enhanced mechanical interlocking. Preliminary experiments to quantify the degree of surface enhancement by BET-measurements with Krypton provide estimates for an enlargement of the true surface area by laser structuring by a factor of 10 to 40. In comparison, LSM measurements, which capture only microstructuring effects, indicate a much less pronounced surface enhancement of ~17% and ~15% for L_{mE} and L_{hE}, respectively. In conclusion, nanostructuring is mainly contributing to the surface enhancement, which increases the number of bonding sites massively for chemical interactions. However, no conclusion concerning the relative contributions of surface enhancement (chemical bonding) versus the nanoscale interlocking can be drawn on the present results. Thus, for Ti15-3/PEEK

bonds a combination of chemical interactions and mechanical interlocking has been evaluated.

For achieving high initial SLS strengths the exact morphology of the structure present on the surface appears to be secondary. In the initial condition a surface structure in the µm-regime (L_{mE}-KEL, $L_{mE\text{-}mV}$-KEL; see also grit blasted structures discussed in Refs. [2, 31, 47]) is already sufficient to increase the joint performance significantly compared to unstructured samples. However, a very pronounced microstructure (e.g., $L_{mE\text{-}lV}$) can reduce the positive effect of structuring on the bonding strength (Fig. 5): due to the characteristics of the "trenches" of the $L_{mE\text{-}lV}$ microstructure (Fig. 2 (e)), air can be trapped within the undercuts during bonding, which may cause a reduced bonding area (see Fig. 15). Moreover, stress concentrations at microstructural surface features may also limit the positive effect of surface structuring.

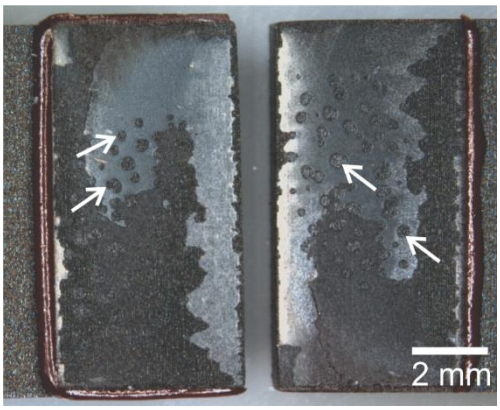

Fig. 15: Fracture surfaces of an SLS specimen (Ti15-3/PEEK) with surface treatment $L_{mE\text{-}lV}$ in initial condition. The arrows mark some of the areas where air was trapped during bonding.

After hydrothermal aging the correlation between surface structures and SLS strength becomes more complex. In the case of unstructured surfaces, the aging resistance drops to 42% for KELLER etched and 32% for untreated samples, respectively (see Fig. 5; Fig. 11), indicating that some degree of chemical bonding is retained even after 7 days in 80 °C hot

H_2O. Interlocking does not account for the bonding in the unstructured samples. Thus, the loss in strength can either be explained by the weakening of the chemical interactions between polymer and substrate in these systems or by a weakening of the polymer. Since PEEK is known for its low water uptake and high strength even after aging [48] and the unstructured SLS specimens failed fully adhesively (see section 3.1.3), the weakening of the chemical interactions is most likely the primary reason for the loss in strength. A hydrothermal conversion of amorphous TiO_2 (to be expected after a non-equilibrium process involving fast quenching like the laser treatment) to crystalline titania modifications [44-46], cannot be ruled out at this point, but this likely would also point to a weakening of the physico-chemical contribution of the bonding. No weak interface and corresponding failure within the oxide film was detected in the fracture surface analysis, i.e., no titania patches or residues were detected on the polymer side of fractured samples with SEM (using the Annular Backscatter and Energy Selective Backscatter detectors as well as Energy-dispersive X-ray spectroscopy), indicating that the failure still occurred at the polymer-oxide interface.

A reordering of the laser-generated surface films to rutile or anatase lattices may still affect the physico-chemical bonding contributions to the joint performance, though, by changing the area density of available surface binding sites (e.g., titanium and oxygen sites), and by changing their local coordination environment. The local structure determines the chemical properties of these binding sites and can lead to a weakening (or strengthening) of the individual bonds (e.g., hydrogen bonding to oxygen lattice atoms and coordinative bonding from PEEK's ketone-oxygen to Ti^{4+} site can be expected to be most relevant). Thus, a conversion of the amorphous laser-generated oxide films may indeed account for the weakening of the physico-chemical bonding. Further investigations will be necessary to study this possibility.

High strengths after aging are only possible with sufficient surface structures, especially with nanostructures. Here the structuring by laser (combination of micro- and nanostructure) is

very effective and leads to high joint strengths after aging: particularly, an open porous, branched nanostructure leads to a high bond strength (L_{hE}: 60 MPa, $L_{mE\text{-}mV}$: 57 MPa, $L_{mE\text{-}lV}$: 56 MPa), (see Fig. 2 (g)-(j) and corresponding residual strengths in Fig. 5). The comparison of the two surface conditions L_{mE} and L_{hE} with very similar microroughness (S_a = 1.1 µm and 1.4 µm, resp.) shows that long-term stability is not only linked to the mere presence of a nanostructure, but also its density and shape: the more compact nanostructure of L_{mE} corresponds to a low aging resistance of 62% while L_{hE} with an open porous, branched nanostructure results in an aging resistance of about 80% (Fig. 2 (g), (h) and Fig. 5). Thus, the morphology of the nanostructure has a significant impact on the aging resistance of the Ti15-3/PEEK joints.

A structured surface alone is not the only key to an aging resistant joint. In fact, not all structured surfaces provide benefits in terms of stability against degradation by H_2O: structuring only in the micrometer regime and to a comparably low degree (e.g., L_{mE}-KEL or grit blasted [31]), i.e. with micro-roughness values below $S_a \leq 1.4$ µm, lead to a poor aging resistance. Apparently, this combination of remaining chemical bonds and interlocking possibilities is insufficient for generating aging resistant Ti15-3/PEEK joints. Hence, these cases evidence the necessity of a nanostructure (see L_{mE} in Fig. 5 compared to L_{mE}-KEL in Fig. 11) for obtaining aging resistant joints.

However, an exception to this finding provides the very pronounced microstructure of $L_{mE\text{-}mV}$-KEL ($S_a \approx 6.2$ µm) samples with residual SLS strengths being comparable to that of L_{mE} samples. Thus, this distinct, trench-like microstructure with undercuts can compete with a nanostructuring, suggesting that mechanical interlocking on the µm-level can compensate for the absence of a nanostructure as well as high stress concentrations to a certain amount.

In contrast, the degree of microstructuring in the presence of a nanostructure appears to exert little influence: if a microstructure was essential for high aging resistance, L_{hE} would not lead

to the highest strength after aging, but the more pronounced microstructures for $L_{mE\text{-}mV}$ or $L_{mE\text{-}lV}$ should provide most benefit. Thus, the presence of a nanostructure itself is obviously the crucial ingredient for a high aging resistance in Ti15-3/PEEK joints.

However, if the presence of an "arbitrary" nanostructure was the only important factor, then the bonding strength and aging resistance of the KOH/H_2O_2 etched samples should be comparable to that of the L_{mE}-KOH specimens, and close to that of the only laser treated ones. Instead, after aging, the KOH samples show only SLS strength values at the level of the unstructured specimens (20 MPa vs. 18 MPa; see Fig. 11), while L_{mE}-KOH has a residual strength of 42 MPa.

In line with the above findings on the different laser generated nanostructures (i.e., L_{mE} and L_{hE} nanostructures; Fig. 2 (g) and (h)), this confirms again that not only the "pure" presence of a nanostructure matters, but also their different appearance or topography, respectively (Fig. 8 (g) and (i)). In conjunction with the observation that the chemistry as judged by XPS is identical in the laser generated and the KOH nanostructures and that infiltration (wetting) has been confirmed in both by TEM and fractography, these differences in strength between all of the nanostructured joints can be traced back to the nanomechanical interlocking. A pronounced, open-porous and branched (L_{hE}) nanostructure such as generated by the pulsed laser pretreatment appears to be essential for strong nanomechanical interlocking and thus long-term stable Ti15-3/PEEK joints [11, 12, 49].

4 Conclusions

A metal-polymer joint has to fulfill several different requirements in order to achieve high strength and aging resistance. A basic requirement for bonding is good wetting of the substrate surface by the polymer arising from attractive physico-chemical interactions. In

addition, the materials of the joint comprising the bond itself, the substrate surface layers and the polymer, must be stable in the operating environment.

These requirements are found to be fulfilled for the investigated Ti15-3/PEEK joints. The results show that the particular surface structures created by surface pretreatments play a fundamental role for the bonding performance of Ti15-3/PEEK joints: The surface enhancement caused by the surface roughness that was created by the laser treatments on the one hand provides more chemical binding sites and on the other hand also increases the possibilities for mechanical interlocking. Importantly, this increase in bonding sites can be linked to the enhanced long-term stability against degrading influences. For a given chemistry (i.e., materials and surface), the particular morphology of the surface is crucial for the bonding performance.

The systematic modification of the type and degree of nano- and microstructuring surface carried out in this investigation revealed that the nanostructuring is significantly more effective in improving the joint properties than the structuring at the µm-level. A pronounced microstructure, e.g., with undercuts for mechanical interlocking, can compensate for the absence of a nanostructure only to a certain degree. The strength reduction of the joints due to aging in 80 °C hot H_2O was mainly caused by degradation of the physico-chemical bonds. Physico-chemical bonds depend on the number of surface sites and are therefore correlated to the true surface area, which is most effectively enhanced by nanoscale structures. Microscopic investigations imply that after breaking of the physico-chemical bonds, interlocking of polymer with the nanostructures is the mechanism providing residual strength or aging resistance, respectively. The presence of water at slightly elevated temperatures may induce a reordering process, i.e., hydrothermal recrystallization, which could indeed account for a weakening of the physico-chemical bonding. Neither major structural changes nor the formation of a weak interface failing in the oxide films was observed on the aged samples.

Hence, while chemistry plays an important role for wetting and infiltration and in the initial, undegraded joint condition, the findings of this work indicate that nanoscale interlocking is the key that determines the aging resistance of the joints.

The pulsed laser pretreatment is found to be a suitable technology for achieving open-porous branched nano-oxide films that satisfy the requirements for achieving long-term stable high strength joints. To what extent this finding can be adapted to other material combinations, especially for other chemical conditions and interactions, has to be investigated further.

Acknowledgements

The authors thank Philipp Watermeyer and Dr. Klemens Kelm (DLR Cologne) for preparing the TEM lamellae and performing the TEM analyses and Iver Lauermann (HZB, Berlin) for providing the XPS facility and valuable assistance. The work was funded as part of programmatic research of the German Aerospace Center (DLR).

References

[1] Baldan A, *Adhesively-bonded joints and repairs in metallic alloys, polymers and composite materials: Adhesives, adhesion theories and surface pretreatment.* J. Mat. Sci., 2004;39:1-49.

[2] Sinmazcelik T, Avcu E, Bora MO, Coban O, *A review: Fibre metal laminates, background, bonding types and applied test methods.* Mat. Design, 2011;32:3671-3685.

[3] Higgins A, *Adhesive bonding of aircraft structures.* Int. J. Adhes. and Adhesiv., 2000;20:367-376.

[4] Davis M, Bond D, *Principles and practices of adhesive bonded structural joints and repairs.* Int. J. Adhes. and Adhesiv., 1999;19:91-105.

[5] Pantelakis S, Tserpes K, eds. *Revolutionizing Aircraft Materials and Processes*. 2020, Springer International Publishing.

[6] Habenicht G, *Applied Adhesive Bonding: A Practical Guide for Flawless Results*. 2009, Weinheim: Wiley-VCH.

[7] Minford JD, *Handbook of Aluminum Bonding Technology and Data*. 1st ed. 1993: CRC Press.

[8] Thrall EW, Shannon RW, *Adhesive Bonding of Aluminum Alloys*. 1985, New York: Routledge.

[9] Park SY, Choi WJ, Choi HS, Kwon H, Kim SH, *Recent Trends in Surface Treatment Technologies for Airframe Adhesive Bonding Processing: A Review (1995-2008).* J. Adhes., 2010;86:192-221.

[10] Venables JD, *Adhesion and Durability of Metal Polymer Bonds.* J. Mat. Sci., 1984;19:2431-2453.

[11] Zimmermann S, Specht U, Spiess L, Romanus H, Krischok S, Himmerlich M et al., *Improved adhesion at titanium surfaces via laser-induced surface oxidation and roughening.* Mat. Sci. Eng. A - Struct. Mat. Prop. Microstruct. and Processing, 2012;558:755-760.

[12] Kurtovic A, Brandl E, Mertens T, Maier HJ, *Laser induced surface nano-structuring of Ti-6Al-4V for adhesive bonding.* Int. J. Adhes. and Adhesiv., 2013;45:112-117.

[13] Palmieri FL, Watson KA, Morales G, Williams T, Hicks R, Wohl CJ et al., *Laser Ablative Surface Treatment for Enhanced Bonding of Ti-6Al-4V Alloy.* Appl. Mat. & Interfaces, 2013;5:1254-1261.

[14] Specht U, Ihde J, Mayer B, *Laser induced nano-porous Ti-O-layers for durable titanium adhesive bonding.* Materialwiss. und Werkstofftechn., 2014;45:1116-1122.

[15] Mertens T, Gammel FJ, Kolb M, Rohr O, Kotte L, Tschoecke S et al., *Investigation of surface pre-treatments for the structural bonding of titanium.* Int. J. Adhes. and Adhesiv., 2012;34:46-54.

[16] Alderliesten RC, Homan JJ, *Fatigue and damage tolerance issues of Glare in aircraft structures.* Int. J. Fatigue, 2006;28:1116-1123.

[17] Baldan A, *Adhesively-bonded joints in metallic alloys, polymers and composite materials: Mechanical and environmental durability performance.* J. Mat. Sci., 2004;39:4729-4797.

[18] Kinloch AJ, *The Science of Adhesion. 2. Mechanics And Mechanisms Of Failure.* J. Mat. Sci., 1982;17:617-651.

[19] Haubrich J, Löbbecke M, Watermeyer P, Wilde F, Requena G, da Silva J, *Buried interfaces – A systematic study to characterize an adhesive interface at multiple scales.* Appl. Surf. Sci., 2018;433:546-555.

[20] Noland JS, *Some Factors for Achieving Environmental Resistance in 120°C Structural Adhesives.* Adhes. Sci. Techn., 1975:413-428.

[21] Harris AF, Beevers A, *The effects of grit-blasting on surface properties for adhesion.* Int. J. Adhes. and Adhesiv., 1999;19:445-452.

[22] Shahid M, Hashim SA, *Effect of surface roughness on the strength of cleavage joints.* Int. J. Adhes. and Adhesiv., 2002;22:235-244.

[23] Ma Z, Zaera F, *Organic chemistry on solid surfaces.* Surf. Sci. Rep., 2006;61:229-281.

[24] Barteau MA, *Organic Reactions at well-defined Oxide Surfaces.* Chem. Rev., 1996;96:1413-1430.

[25] Kromer R, Costil S, Cormier J, Courapied D, Berthe L, Peyre P et al., *Laser surface patterning to enhance adhesion of plasma sprayed coatings.* Surf. & Coat. Techn., 2015;278:171-182.

[26] Baburaj EG, Starikov D, Evans J, Shafeev GA, Bensaoula A, *Enhancement of adhesive joint strength by laser surface modification.* Int. J. Adhes. and Adhesiv., 2007;27:268-276.

[27] He P, Chen K, Yu B, Yue CY, Yang J, *Surface microstructures and epoxy bonded shear strength of Ti6Al4V alloy anodized at various temperatures.* Compos. Sci. Techn., 2013;82:15-22.

[28] Zheng R, Lin J, Wang P-C, Zhu C, Wu Y, *Effect of adhesive characteristics on static strength of adhesive-bonded aluminum alloys.* Int. J. Adhes. and Adhesiv., 2015;57:85-94.

[29] Assefpour-Dezfuly M, Vlachos C, Andrews EH, *Oxide morphology and adhesive bonding on titanium surfaces.* J. Mat. Sci., 1984;19:3626-3639.

[30] Chawla KK, *Composite Materials - Science and Engineering*. 2nd ed. 1998: Springer Science & Business Media.

[31] Molitor P, Barron V, Young T, *Surface treatment of titanium for adhesive bonding to polymer composites: a review.* Int. J. Adhes. and Adhesiv., 2001;21:129-136.

[32] Kinloch AJ, Taig CM, *The adhesive bonding of thermoplastic composites.* J. Adhes., 1987;21:291-302.

[33] Haubrich J, Kaxiras E, Friend CM, *The Role of Surface and Subsurface Point Defects for Chemical Model Studies on TiO_2: A First-Principles Theoretical Study of Formaldehyde Bonding on Rutile TiO_2(110).* Chem.- A Eur. J., 2011;17:4496-4506.

[34] Henderson MA, *Acetone and water on TiO_2(110): competition for sites.* Langmuir, 2005;21:3443-50.

[35] Márquez A, Plata J, Fdez Sanz J, *Role of Coverage and Surface Oxidation Degree in the Adsorption of Acetone on TiO2 (110). A Density Functional Study.* J. Phys. Chem. C, 2009;113.

[36] Tougaard S, *Quantitative analysis of the inelastic background in surface electron spectroscopy.* Surf. Interf. Anal., 1988;11:453-472.

[37] Wang Q, Biener J, Guo X-C, Farfan-Arribas E, Madix RJ, *Reactivity of Stoichiometric and Defective TiO_2(110) Surfaces toward DCOOD Decomposition.* J. Phys. Chem. B, 2003;107:11709-11720.

[38] Pouilleau J, Devilliers D, Garrido F, Durand-Vidal S, Mahé E, *Structure and composition of passive titanium oxide films.* Materials Science and Engineering: B, 1997;47:235-243.

[39] Ketteler G, Yamamoto S, Bluhm H, Andersson K, Starr DE, Ogletree DF et al., *The Nature of Water Nucleation Sites on TiO2(110) Surfaces Revealed by Ambient Pressure X-ray Photoelectron Spectroscopy.* J. Phys. Chem. C, 2007;111:8278-8282.

[40] Moulder JF, Stickle WF, Sobol PE, Bomben KD, *Handbook of X-ray photoelectron spectroscopy*. 1995.

[41] Haubrich J, Quiller RG, Benz L, Liu Z, Friend CM, *In Situ Ambient Pressure Studies of the Chemistry of NO_2 and Water on Rutile TiO_2(110).* Langmuir, 2010;26:2445-2451.

[42] Crist BV, *XPS Handbook of the Elements and Native Oxides*. 1999.

[43] Alexander MR, Beamson G, Bailey P, Noakes TCQ, Skeldon P, Thompson GE, *The distribution of hydroxyl ions at the surface of anodic alumina.* Surf. Interf. Anal., 2003;35:649-657.

[44] Matthews A, *The crystallization of anatase and rutile from amorphous titanium dioxide under hydrothermal conditions.* Am. Mineralogist, 1976;61:419-424.

[45] Yanagisawa K, Ovenstone J, *Crystallization of Anatase from Amorphous Titania Using the Hydrothermal Technique: Effects of Starting Material and Temperature.* J. Phys. Chem. B, 1999;103:7781-7787.

[46] Mitchell DRG, Triani G, Zhang Z, *Hydrothermal crystallization of amorphous titania films deposited using low temperature atomic layer deposition.* Thin Solid Films, 2008;516:8414-8423.

[47] Critchlow GW, Brewis DM, Emmony DC, Cottam CA, *Initial investigation into the effectiveness of CO_2-laser treatment of aluminium for adhesive bonding.* Int. J. Adhes. and Adhesiv., 1995;15:233-236.

[48] VICTREX, *Materials Properties Guide - A comprehensive review of the materials properties of VICTREX PEEK high performance polymer*.

[49] Löbbecke M, *Einflussfaktoren und deren Auswirkung auf das Adhäsions- und Alterungsverhalten von Titan-Polymer-Klebungen, Ph.D. (Dr.-Ing.) thesis, Faculty of Mechanical Engineering*. 2019, Ruhr-University Bochum.